Journal of Solid State Chemistry **167,** 107–112 (2002)
doi:10.1006/jssc.2002.9626

New Compounds of the $ThCr_2Si_2$-Type and the Electronic Structure of CaM_2Ge_2 (M: Mn–Zn)

Christian Kranenberg,* Dirk Johrendt,* Albrecht Mewis,*,[1] Rainer Pöttgen,† Gunter Kotzyba,† Henning Trill,‡ and Bernd D. Mosel‡

*Institut für Anorganische Chemie und Strukturchemie II der Heinrich-Heine-Universität, Universitätsstraße 1, D-40225 Düsseldorf, Germany; †Institut für Anorganische und Analytische Chemie, Universität Münster, Wilhelm-Klemm-Straße 8, D-48149 Münster, Germany; and ‡Institut für Physikalische Chemie, Universität Münster, Schloßplatz 4/7, D-48149 Münster, Germany

Received February 12, 2002; in revised form April 4, 2002; accepted April 19, 2002

Two new compounds were synthesized by heating mixtures of the elements at 975–1025 K and characterized by single-crystal X-ray methods. $CaZn_2Si_2$ ($a = 4.173(2)$ Å, $c = 10.576(5)$ Å) and $EuZn_2Ge_2$ ($a = 4.348(2)$ Å, $c = 10.589(9)$ Å) crystallize in the $ThCr_2Si_2$-type structure (space group $I4/mmm$; $Z = 2$). Magnetic susceptibility measurements of $EuZn_2Ge_2$ show Curie–Weiss behavior with a magnetic moment of 7.85(5) μ_B/Eu and a paramagnetic Curie temperature of 10(1) K. $EuZn_2Ge_2$ orders antiferromagnetically at $T_N = 10.0(5)$ K and undergoes a metamagnetic transition at a low critical field of about 0.3(2) T. The saturation magnetization at 2 K and 5.5 T is 6.60(5) μ_B/Eu. ^{151}Eu Mössbauer spectroscopic experiments show one signal at 78 K at an isomer shift of −11.4(1) mm/s and a line width of 2.7(1) mm/s compatible with divalent europium. At 4.2 K full magnetic hyperfine field splitting with a field of 26.4(4) T is detected. The already known compounds CaM_2Ge_2 (M: Mn–Zn) also crystallize in the $ThCr_2Si_2$-type structure. Their MGe_4 tetrahedra are strongly distorted with M = Ni and nearly undistorted with M = Mn or Zn. According to LMTO electronic band structure calculations, the distortion is driven by a charge transfer from M–Ge antibonding to bonding levels.

Key Words: **silicide; germanide; crystal structure; magnetism; ^{151}Eu Mössbauer spectroscopy; electronic structure.**

INTRODUCTION

The well-known $ThCr_2Si_2$-type, first reported by Ban and Sikirica in 1965 (1), is the crystal structure with the highest number of representatives (2). The main reasons for this are its possibility to adapt to strongly different atomic sizes as well as to a wide range of electron counts. Many $ThCr_2Si_2$ compounds have interesting physical properties such as superconductivity, e.g., in $LaRu_2P_2$ (3), mixed valency, e.g., in $EuNi_2P_2$ (4), as well as a wide range of magnetic properties (5–7). In the formulation AM_2X_2, A generally is a alkaline- or rare-earth metal, M mostly a transition metal, and X an element from the groups 13–16. The structure is built up by negatively charged layers of MX_4 tetrahedra and positively charged A layers, alternately stacked along [001]. The MX_4 layers contain strong covalent M–X bonds and weaker M–M interactions, while the bonding between A and the layers is rather ionic. With LMTO band structure calculations, we have shown (8) that in ternary phosphides neither a covalent nor metallic or ionic bonding scheme alone can give an appropriate description. All three kinds of bonding are present in these compounds. The interrelations between them can cause instabilities resulting in first- and second-order phase transitions induced by temperature, pressure, and substitution, respectively. The phase transitions are mostly accompanied by strong changes of the lattice parameters and particularly of the P–P distance between the layers of MP_4 tetrahedra (9–14).

In the present paper, we report about the preparation and crystal structure of $CaZn_2Si_2$ and $EuZn_2Ge_2$ as well as magnetic measurements and Mössbauer spectroscopic experiments of the europium compound. In order to understand the unusual changes in the lattice parameters of CaM_2Ge_2 with M = Mn–Zn, we present an analysis of chemical bonding based on LMTO band-structure calculations.

EXPERIMENTAL SECTION

$CaZn_2Si_2$ and $EuZn_2Ge_2$ were synthesized by direct reaction of the elements in corundum crucibles, sealed in quartz glass tubes under dry argon. Reaction temperatures were 975 K for 20 h. The first inhomogeneous products

[1] To whom correspondence should be addressed. Fax: +49-211-811-4146. E-mail: albrecht.mewis@uni-duesseldorf.de, johrendt@uni-duesseldorj.de.

0022-4596/02 $35.00

were homogenized and annealed twice at 1025 K for 50 h. The resulting gray powders slowly decompose when exposed to air. Experiments to synthesize additional compounds of trivalent rare-earth metals failed. Instead of the expected compounds, the germanides $Ln_4Zn_5Ge_6$ (*Ln:* Gd, Tm, Lu) (15) and other not identified phases were formed.

X-ray powder diagrams (HUBER G600, Cu$K\alpha_1$, calibrated with Si) could be indexed tetragonally with lattice constants typical for $ThCr_2Si_2$ compounds. Single crystal data were collected with an automated four–circle diffractometer STOE AED-2 (Mo$K\alpha_1$, graphite monochromator). Absorption effects were corrected by acquiring ψ–scan data; structure refinements were performed with the SHELXL-97 (16) package.

The electrical resistivity of $EuZn_2Ge_2$ was measured on a polycrystalline pellet (cold pressed with 40 kN, annealed at 1073 K for 15 h) using a four-probe dc current reversal technique between 8 and 320 K.

The magnetic susceptibilities of $EuZn_2Ge_2$ were determined with a SQUID magnetometer (MPMS, Quantum Design, Inc.) between 2 and 300 K with magnetic flux densities up to 5.5 T. The 21.53 keV transition of ^{151}Eu with an activity of 130 MBq (2% of the total activity of a ^{151}Sm:EuF_3 source) was used for the Mössbauer spectroscopic investigations. The measurements were carried out with a helium bath cryostat. The temperature of the absorber could be varied from 4.2 to 300 ± 0.5 K. The source was kept at room temperature. The sample was placed within a PVC container at a thickness corresponding to about 10 mg Eu/cm^2.

Self-consistent band-structure calculations were performed using the LMTO method in its scalar relativistic version (program LMTO-ASA 47) (17). A detailed description may be found elsewhere (18,19). Reciprocal space integrations were performed with the tetrahedron method using 149 irreducible *k*–points within the Brillouin zone (20). The basis sets consisted of 4*s*, 3*d* orbitals for Ca; 4*s*, 4*p* for Ge; 4*s*, 4*p*, 3*d* for Mn, Co, Ni, Cu and Zn. The 4*p* orbitals for Ca and 4*d* for Ge were treated by the down-folding technique (21). To achieve space filling within the atomic sphere approximation, interstitial spheres are introduced to avoid too large overlap of the atom-centered spheres. The empty sphere positions and radii were calculated using an automatic procedure developed by Krier *et al.* (22). We did not allow an overlap of more than 15% for any two atom-centered spheres.

RESULTS AND DISCUSSION

$CaZn_2Si_2$ and $EuZn_2Ge_2$

Precession photographs of $CaZn_2Si_2$ and $EuZn_2Ge_2$ showed exclusively reflections of a tetragonal body-centered unit cell. The systematic extinctions and unit cell dimensions suggested isotypism to the $ThCr_2Si_2$-type (space group *I*4/*mmm*). Another ternary derivative of the $BaAl_4$ structure with similar lattice parameters is the $CaBe_2Ge_2$-type (space group *P*4/*nmm*). In the case of $EuZn_2Ge_2$, it is almost impossible to discriminate with X-ray diffraction between the two structures. The main problem is that the lattice-ordering scheme is determined by the site distribution of Zn and Ge, which are nearly isoelectronic. However, from geometric reasons the $CaBe_2Ge_2$-type can only be expected with *A* and *X* elements of relative small and big atomic size, respectively (23). Refinements of the single crystal data of both compounds converged rapidly with the atomic positions of $CaZn_2Ge_2$ ($ThCr_2Si_2$-type) (24) as starting parameters. Crystallographic data, final coordinates, and anisotropic displacement parameters are summarized in Table 1; selected bond lengths and angles are compiled in Table 2.

$EuZn_2Ge_2$ fits well in the series of isotypic compounds AZn_2Ge_2 with *A* = Ca, Sr (24, 25), Yb (26), and Ba (27), while $CaZn_2Si_2$ is the first zinc silicide of alkaline-earth metals crystallizing in the $ThCr_2Si_2$-type. The crystal structure of both compounds is presented in Fig. 1. In $EuZn_2Ge_2$, the Zn–Ge distance is 2.59 Å, slightly longer than the sum of the covalent radii (2.46 Å) (28). The Ge–Ge bond length along [001] of 2.47 Å corresponds to the distance in cubic germanium, which is also valid for the other isotypic zinc germanides AZn_2Ge_2. The distances range from 2.46 Å in $YbZn_2Ge_2$ to 2.56 Å in $BaZn_2Ge_2$.

TABLE 1
Crystallographic Data of AZn_2X_2 (*A*: Ca, Eu; *X*: Si, Ge)

Formula	$CaZn_2Si_2$	$EuZn_2Ge_2$
Space group	*I*4/*mmm*	*I*4/*mmm*
a (Å)	4.173(2)	4.348(2)
c (Å)	10.576(5)	10.589(9)
c/*a*	2.534	2.435
Volume (Å^3)	184.2(2)	200.2(2)
Z	2	2
Calc. Density	4.093 g/cm^3	7.099 g/cm^3
2θ range	$3^\circ \le 2\theta \le 80^\circ$	$3^\circ \le 2\theta \le 80^\circ$
Total no. reflections	695	743
Independent reflections	204	217
R_1 ($I > 2\sigma(I)$)	0.048	0.065
wR_2 (all data)	0.152	0.119
Atomic parameters		
A (0, 0, 0)		
U_{11}	102(12)	72(6)
U_{33}	130(16)	135(8)
Zn (0, $\frac{1}{2}$, $\frac{1}{4}$)		
U_{11}	148(7)	99(8)
U_{33}	139(8)	95(12)
X (0, 0, *z*)	$z = 0.3883(4)$	$z = 0.3833(3)$
U_{11}	54(10)	115(8)
U_{33}	19(12)	92(12)

TABLE 2
Interatomic Distances (Å) and Bond Angles (deg) for AZn_2X_2 (A: Ca, Eu; X: Si, Ge)

Formula	$CaZn_2Si_2$	$EuZn_2Ge_2$
A–8 X	3.179(2)	3.314(2)
8 Zn	3.368(1)	3.426(2)
Zn–4 X	2.548(2)	2.592(2)
4 Zn	2.951(1)	3.075(1)
$\angle X$–Zn–X	109.9(1)	114.0(1)
X–1 X	2.363(8)	2.472(6)

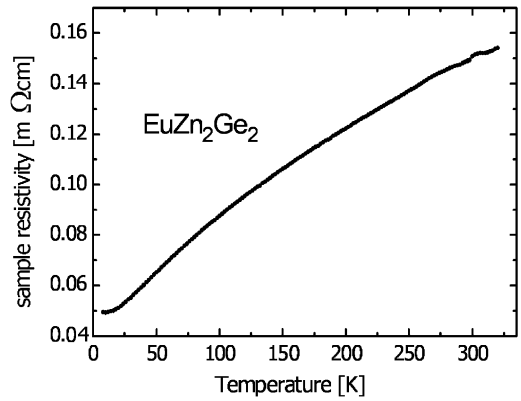

FIG. 2. Temperature dependence of the electrical resistivity of $EuZn_2Ge_2$.

This can be realized in spite of the growing atomic size of A, because the Zn–Zn distance increases from 2.95 Å in $YbZn_2Ge_2$ to 3.20 Å in $BaZn_2Ge_2$, while the Zn–Ge bond lengths remain 2.56–2.64 Å and the $ZnGe_4$ tetrahedra become flatter. The alkaline-earth metal in the three-dimensional covalent (Zn, Ge) framework is coordinated by germanium atoms only, while the A–Zn distances are much longer than the sums of the radii (A: atomic radius (KZ 12); Zn: covalent radius). The bond lengths of $CaZn_2Si_2$ are comparable with those of the germanides. The Si–Si bond length of 2.36 Å is short (covalent radius of Si: 1.17 Å), but it is remarkable that the Zn–Si distance of 2.55 Å distinctly exceeds the sum of covalent radii (2.39 Å). We also have synthesized $SrZn_2Si_2$ and indexed the X-ray powder diagram tetragonally with the lattice constants $a = 4.326(1)$ Å and $c = 10.351(3)$ Å. But unfortunately, we found no suitable single crystal to confirm the supposed $ThCr_2Si_2$-type structure.

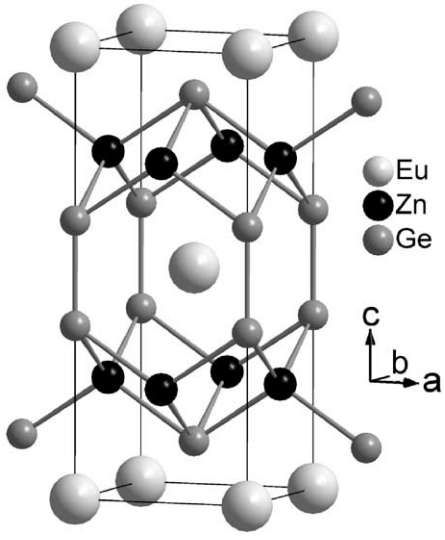

FIG. 1. Crystal structure of $EuZn_2Ge_2$ ($ThCr_2Si_2$-type).

The temperature dependence of the electrical resistivity of $EuZn_2Ge_2$, shown in Fig. 2, shows the metallic state of the germanide though the formula $Eu^{2+}(Zn_2)^{4+}(Ge_2)^{6-}$ fulfills Zintl's concept.

The inverse magnetic susceptibility of $EuZn_2Ge_2$ as a function of temperature is presented in Fig. 3. Above 40 K, we observe Curie–Weiss behavior with a magnetic moment of 7.85(5) μ_B/Eu, close to the value of 7.94 μ_B for the free Eu^{2+} ion (29). The paramagnetic Curie temperature (Weiss constant) of 10(1) K was determined by linear extrapolation of the $1/\chi$ vs. T plot to $1/\chi = 0$.

Antiferromagnetic ordering of the europium magnetic moments at the Néel temperature of $T_N = 10.0(5)$ K is obvious from the low-temperature 0.1 T data (inset of Fig. 3). The magnetization vs. external magnetic flux density at 2 and 50 K is displayed in Fig. 4. At 50 K the magnetization curve is almost linear as expected for a paramagnetic material. This is different at 2 K. Up to the critical field of about 0.3(2) T, we also observe a nearly

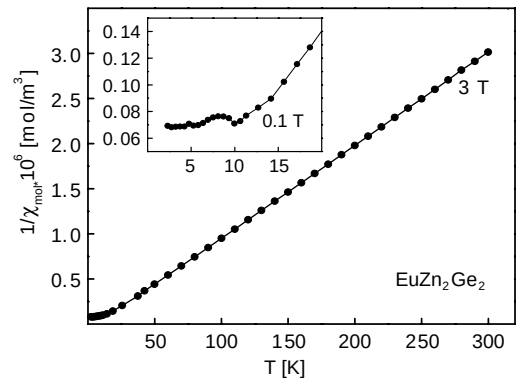

FIG. 3. Temperature dependence of the reciprocal magnetic susceptibility of $EuZn_2Ge_2$ measured at an external field of 3 T. The low-temperature behavior (0.1 T data) is presented in the inset.

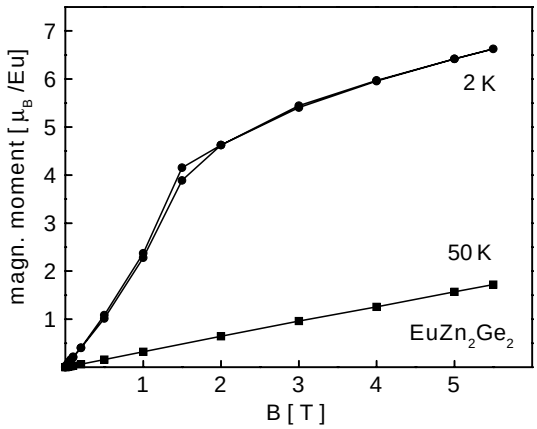

FIG. 4. Magnetic moment vs. external magnetic flux density for $EuZn_2Ge_2$ at 2 and 50 K.

linear increase of the magnetization, but then a stronger increase. This magnetization behavior is due to a metamagnetic (antiparallel to parallel spin alignment) transition as is frequently observed for similar europium intermetallics (30). The metamagnetic transition, however, is not very pronounced. At the highest obtainable magnetic field of 5.5 T the magnetization is 6.60(5) μ_B/Eu, in good agreement with the maximal value of 7.0 μ_B/Eu according to $g \times J$ (29). We have thus almost reached a full parallel spin alignment.

The ^{151}Eu Mössbauer spectra at 78, 15, 10, and 4.2 K are presented in Fig. 5 together with transmission integral fits. An Eu^{3+} impurity around an isomer shift of $\delta = 1.1$ mm/s was detected in all spectra and included in the fits as a simple Lorentzian component. The fractional area of the Eu^{3+} component is about 4% and most likely resulted from a partial oxidation of the sample.

At 78 K, well above the Néel temperature, the spectrum is well reproduced by a single Eu^{2+} site with an isomer shift of $-11.4(1)$ mm/s and an experimental line width of $\Gamma = 2.7(1)$ mm/s. The onset of magnetic ordering in $EuZn_2Ge_2$ is detected in the Mössbauer experiment already at about 15 K through a beginning broadening ($\Gamma = 2.8(1)$ mm/s) of the signal (Fig. 5). The ordering temperature determined by ^{151}Eu Mössbauer spectroscopy is slightly higher than the Néel temperature determined through the susceptibility measurements. Such an effect is frequently observed for europium intermetallics (30, 31). At 10 K, we already observe a significant degree of hyperfine field splitting, which is complete at 4.2 K. The corresponding fitting parameters are $\delta = -11.4(1)$ mm/s, $\Gamma = 2.6(3)$ mm/s, and $B = 26.4(4)$ T.

At this point it is interesting to discuss the physical properties of $EuZn_2Ge_2$ in line with the other EuM_2Ge_2 germanides (29). In this family of $ThCr_2Si_2$-type compounds, $EuZn_2Ge_2$ has the lowest magnetic-ordering temperature and the most negative isomer shift. Similar negative isomer shifts are typically observed for such electrovalent europium intermetallics, e.g., EuZnGe or EuAuP (30), where the ionic formula splitting formally leads to $Eu^{2+}Zn^{2+}Ge^{4-}$ and $Eu^{2+}Au^{+}P^{3-}$ as requested by Zintl's concept. This holds also true for $Eu^{2+}(Zn_2)^{4+}(Ge_2)^{6-}$.

During the preparation of this paper, *Rogl* and coworkers reported about $EuZn_2Ge_2$ with $CaBe_2Ge_2$-structure (32), synthesized in a zinc flux. This structure is rather unexpected for $EuZn_2Ge_2$ from electronic as well as from atom size arguments. Probably, the large excess of zinc somehow stabilizes the tetragonal primitive variant, which differs also from the body centered one by a longer lattice parameter ($c = 10.79$ Å instead of 10.59 Å) and a lower Néel temperature ($T_N = 7.5$ instead of 10 K).

The Electronic Structure of CaM_2Ge_2 (M = Mn–Zn)

The compounds CaM_2Ge_2 with M = Mn, Co, Ni (25), Cu, and Zn (26) crystallize in the $ThCr_2Si_2$-type. The lattice constants along this series show remarkable changes: c decreases from Mn to Ni by 0.9 Å and then increases to Zn almost by the same amount. In order to understand this behavior, we have investigated the electronic structures of these compounds by LMTO band-structure calculations. The decrease of c is caused by a distortion of the MGe_4 tetrahedra (see Table 3), which evidently has electronic reasons. Therefore, we compare the band structure of $CaNi_2Ge_2$ with that of a fictitious $CaNi_2Ge_2$ with undistorted $NiGe_4$ tetrahedra. To calculate the latter one, the lattice constant a and the Ge–Ge distance were kept

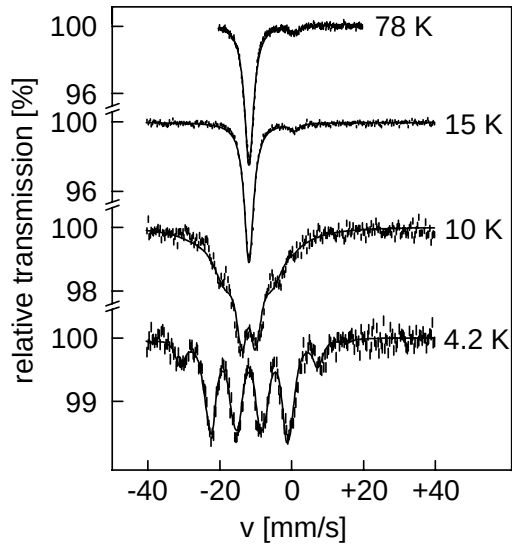

FIG. 5. Experimental and simulated ^{151}Eu Mössbauer spectra of $EuZn_2Ge_2$.

TABLE 3
Lattice Parameters, Atomic Distances (Å), and Tetrahedral Angles (deg) of CaM_2Ge_2 (M: Mn–Zn)

Compound	a	c	d_{M-Ge}	d_{M-M}	d_{Ge-Ge}	∠Ge–M–Ge	Ref.
$CaMn_2Ge_2$	4.17	10.88	2.50	2.95	2.60	111.97	(25)
$CaCo_2Ge_2$	4.00	10.33	2.35	2.83	2.65	115.99	(25)
$CaNi_2Ge_2$	4.08	9.98	2.36	2.88	2.61	119.59	(25)
$CaCu_2Ge_2$	4.14	10.23	2.45	2.93	2.48	114.94	(26)
$CaZn_2Ge_2$	4.21	10.85	2.57	2.98	2.47	109.94	(26)

fixed, while the value of c was increased to 10.95 Å. Fig. 6 shows the calculated band structures of both compounds along the lines $Z(0, 0, \pi/c) \rightarrow \Gamma(0, 0, 0) \rightarrow X(\pi/a, \pi/a, 0) \rightarrow z$ $(\pi/a, 0, 0) \rightarrow \Gamma(0, 0, 0)$. Because of the body-centered lattice, the point Z is equivalent with z at the top/bottom of the neighboring Brillouin zones. Significant differences discern at the Z points. One band, marked in Fig. 6 as 1 at Z (1a at z), is pushed above the Fermi level by the distortion of the tetrahedra and becomes partially emptied. In order to present a more chemical view of this electronic level, we have calculated the contribution of the band 1 states around Z to the electron density, as shown in Fig. 7. The strong Ge–Ge bonding character is clearly visible, and from the vanishing density between Ni and Ge, the Ni–Ge antibonding character is evident. Since the total number of occupied states must be constant, another band has to move below the Fermi level. This happens mainly around the X point, where the band marked with 2 gets more filled by the distortion (Fig. 6). As the orbital vector analysis shows, this band has mainly Ni–Ge bonding character. From this, we infer that a charge transfer from antibonding to bonding Ni–Ge states, which clearly lowers the total energy of the structure, triggers the distortion of the $NiGe_4$-tetrahedra.

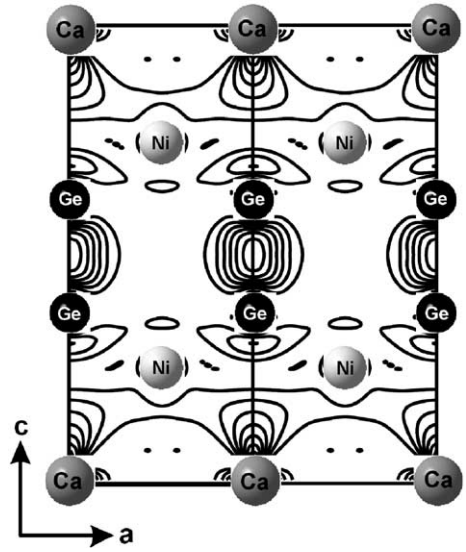

FIG. 7. Partial electron density of $CaNi_2Ge_2$ at point Z (values (ρ) from 0 to 0.02 in steps of 0.002).

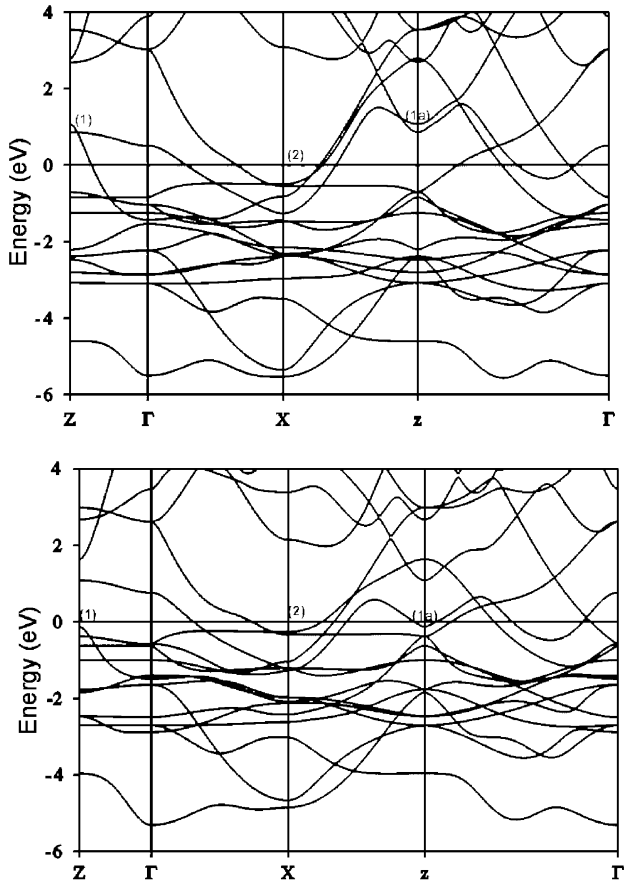

FIG. 6. Band structure of $CaNi_2Ge_2$ with distorted (top) and undistorted (bottom) $NiGe_4$ tetrahedra. The energy zero is taken at the Fermi level.

The band structure of $CaCo_2Ge_2$ is essentially the same as for the nickel compound, but the band filling is lower because of the smaller number of $3d$ electrons. The concerning Co–Ge antibonding bands are less filled from the outset, therefore a smaller distortion of the tetrahedra is sufficient to reach the stabilization effect described above.

The magnetic properties of manganese in $CaMn_2Ge_2$ (33) required spin-polarized calculations. We assumed a ferromagnetic spin alignment to keep the symmetry. Despite the magnetic splitting, the results are similar to the cobalt compound, but now the concerning Mn–Ge antibonding band is already empty and therefore no driving force for a distortion exists.

Significant differences in the band structure occur when copper is introduced (Fig. 8). Because of the $3d^{10}$ configuration, the Cu $3d$-shell interacts much weaker with the Ge

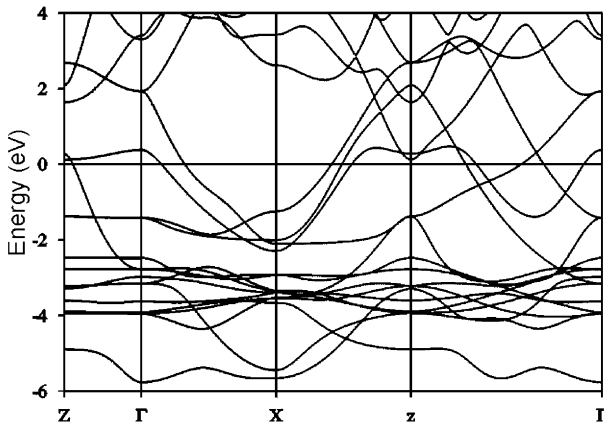

FIG. 8. Band structure of $CaCu_2Ge_2$. The energy zero is taken at the Fermi level.

s and *p* levels, which changes the bonding character of the bands. Particularly, the above-mentioned Cu–Ge antibonding and Ge–Ge bonding states (Fig. 7) around *Z* and *z* have almost purely Ge–Ge bonding and only weak Cu–Ge antibonding character. Again the distortion of the tetrahedra pushes Cu–Ge antibonding states at the top of the band (near *Z* and *z*) above the Fermi level. But the major part of this band remains occupied and stronger Ge–Ge bonding is expected. Indeed the Ge–Ge distance in $CaCu_2Ge_2$ of 2.48 Å is shortest in this series.

Finally, the $ZnGe_4$ tetrahedra in $CaZn_2Ge_2$ are undistorted. This is because the closed Zn 3*d* shell interacts virtually not with other orbitals. Consequently, no Zn–Ge antibonding states exist near the Fermi level and a distortion of the $ZnGe_4$ tetrahedra would not make any gain in energy.

ACKNOWLEDGMENTS

We are grateful to Prof. W. Jeitschko and Prof. H. Eckert for use of their SQUID magnetometer and the Mössbauer equipment. The Fonds der Chemischen Industrie and the Deutsche Forschungsgemeinschaft supported this work financially.

REFERENCES

1. Z. Ban and M. Sikirica, *Acta Crystallogr.* **18,** 594 (1965).
2. P. Villars and L. D. Calvert, "Pearson's Handbook of Crystallographic Data for Intermetallic Phases," 2nd ed. and desk ed. ASM International, Materials Park, OH, 1991 and 1997.
3. W. Jeitschko, R. Glaum, and L. Boonk, *J. Solid State Chem.* **69,** 93 (1987).
4. R. Nagarajan, E. V. Sampathkumaran, L. C. Gupta, R. Vijayaraghavan, V. Prabhabwalkar, and B. Padalia, *Phys. Lett. A* **84,** 275 (1981).
5. K. A. Gschneider and L. Eyring, "Handbook of Physics and Chemistry of Rare Earth," Vol. 12, p. 133. Elsevier, Amsterdam, 1989.
6. M. Reehuis and W. Jeitschko, *J. Phys. Chem. Solids* **51,** 961 (1990).
7. B. Ni, M. M. Abd-Elmeguid, H. Micklitz, J. P. Sanchez, P. Vulliet, and D. Johrendt, *Phys. Rev. B* **63,** 100102-1 (2001).
8. D. Johrendt, C. Felser, O. Jepsen, O. K. Andersen, A. Mewis, and J. Rouxel, *J. Solid State Chem.* **130,** 254 (1997).
9. A. Wurth, D. Johrendt, A. Mewis, C. Huhnt, G. Michels, M. Roepke, and W. Schlabitz, *Z. Anorg. Allg. Chem.* **623,** 1418 (1997).
10. V. Keimes, D. Johrendt, A. Mewis, C. Huhnt, and W. Schlabitz, *Z. Anorg. Allg. Chem.* **623,** 1699 (1997).
11. C. Huhnt, G. Michels, M. Roepke, W. Schlabitz, A. Wurth, D. Johrendt, and A. Mewis, *Physica B* **240,** 26 (1997).
12. C. Huhnt, W. Schlabitz, A. Wurth, A. Mewis, and M. Reehuis, *Phys. Rev. B* **56,** 13796 (1997).
13. C. Huhnt, W. Schlabitz, A. Wurth, A. Mewis, and M. Reehuis, *Physica B* **252,** 44 (1998).
14. V. Keimes, A. Hellmann, D. Johrendt, and A. Mewis, *Z. Anorg. Allg. Chem.* **624,** 830 (1998).
15. C. Kranenberg, D. Johrendt, and A. Mewis, *Z. Anorg. Allg. Chem.* **627,** 539 (2001).
16. G. M. Sheldrik, "SHELXL-97 Program for Crystal Structure Refinement," Universität Göttingen, Germany, 1997.
17. O. K. Andersen, Tight-Binding LMTO Vers. 47, Max-Planck-Institut für Festkörperforschung, Stuttgart, 1994.
18. H. L. Skriver, "The LMTO Method," Springer-Verlag, Berlin, 1984.
19. O. Jepsen, M. Snob, and O. K. Andersen, "Linearized Band-Structure Methods in Electronic Band-Structure and its Applications," Springer Lecture Notes, Springer-Verlag, Berlin, 1987.
20. O. K. Andersen and O. Jepsen, *Solid State Commun.* **9,** 1763 (1971).
21. W. R. L. Lambrecht and O. K. Andersen, *Phys. Rev. B* **34,** 2439 (1986).
22. G. Krier, O. Jepsen, and O. K. Andersen, unpublished.
23. A. Mewis, *Z. Anorg. Allg. Chem.* **536,** 7 (1986).
24. B. Eisenmann, N. May, W. Müller, H. Schäfer, A. Weiss, J. Winter, and G. Ziegleder, *Z. Naturforsch.* **25b,** 1350 (1970).
25. W. Dörrscheidt, N. Niess, and H. Schäfer, *Z. Naturforsch.* **31b,** 890 (1976).
26. A. Grytsiv, A. Leithe-Jasper, H. Flandorfer, P. Rogl, K. Hiebl, C. Godart, and T. Velikanova, *J. Alloys Compds.* **266,** 7 (1998).
27. D. M. Proserpio, G. Artioli, S. Mulley, G. Chacon, and C. Zheng, *Chem. Mater.* **9,** 1463 (1997).
28. L. Pauling, "Die Natur der Chemischen Bindung," p. 379, Verlag Chemie, Weinheim, 1976.
29. A. Szytuła and J. Leciejewicz, "Handbook of Crystal Structures and Magnetic Properties of Rare Earth Intermetallics," CRC Press, Boca Raton, Florida, 1994.
30. R. Pöttgen and D. Johrendt, *Chem. Mater.* **12,** 875 (2000).
31. R. Müllmann, B. D. Mosel, H. Eckert, G. Kotzyba, and R. Pöttgen, *J. Solid State Chem.* **137,** 174 (1998).
32. A. Grytsiv, D. Kaczorowski, A. Leithe-Jasper, P. Rogl, C. Godart, M. Potel, and H. Noël, *J. Solid State Chem.* /www.idealibrary.com/links/doi/10.1006/jssc.2001.9350
33. B. Malaman, G. Venturini, R. Welter, and E. Ressouche, *J. Alloys Compds.* **210,** 209 (1994).